Hindawi Publishing Corporation
Journal of Nanomaterials
Volume 2015, Article ID 308465, 9 pages
http://dx.doi.org/10.1155/2015/308465

Research Article

Sensitivity of Mesoporous $CoSb_2O_6$ Nanoparticles to Gaseous CO and C_3H_8 at Low Temperatures

Héctor Guillén-Bonilla,[1,2] Lorenzo Gildo-Ortiz,[1] M. de la L. Olvera-Amador,[3] Jaime Santoyo-Salazar,[4] Verónica M. Rodríguez-Betancourtt,[5] Alex Guillen-Bonilla,[5] and Juan Reyes-Gómez[2]

[1]*Facultad de Ciencias Químicas, Universidad de Colima, 28400 Coquimatlán, COL, Mexico*
[2]*Facultad de Ciencias, Universidad de Colima, 28045 Colima, COL, Mexico*
[3]*Departamento de Ingeniería Eléctrica-SEES, Centro de Investigación y de Estudios Avanzados del Instituto Politécnico Nacional, 07360 México, DF, Mexico*
[4]*Departamento de Física, Centro de Investigación y de Estudios Avanzados del Instituto Politécnico Nacional, 07360 México, DF, Mexico*
[5]*Centro Universitario de Ciencias Exactas e Ingenierías, Universidad de Guadalajara, 44410 Guadalajara, JAL, Mexico*

Correspondence should be addressed to Héctor Guillén-Bonilla; hguillenbonilla@gmail.com

Received 14 November 2014; Accepted 7 January 2015

Academic Editor: Rakesh K. Joshi

Copyright © 2015 Héctor Guillén-Bonilla et al. This is an open access article distributed under the Creative Commons Attribution License, which permits unrestricted use, distribution, and reproduction in any medium, provided the original work is properly cited.

Mesoporous $CoSb_2O_6$ nanoparticles, synthesized through a nonaqueous method (using cobalt nitrate, antimony trichloride, ethylenediamine, and ethanol as a solvent), were tested to establish their sensitivity to CO and C_3H_8 atmospheres at relatively low temperatures. The precursor material was dried at 200°C and calcined at 600°C. X-ray diffraction and scanning electron microscopy were employed to verify the existence of crystal phases ($P4_2/mnm$) and the morphology of this trirutile-type $CoSb_2O_6$ oxide. Pyramidal and cubic shaped crystals (average size: 41.1 nm), embedded in the material's surface, were identified. Mesopores (average size: 6.5 nm) on the nanoparticles' surface were observed by means of transmission electron microscopy. The best sensitivity of the $CoSb_2O_6$ in a CO atmosphere was at the relatively low temperatures of 250 and 350°C, whereas, in a C_3H_8 atmosphere, the sensitivity increased uniformly with temperature. These results encourage using the $CoSb_2O_6$ nanoparticles as gas sensors.

1. Introduction

In recent years, nanoscience and nanotechnology have had a huge impact on many fields of scientific research. New materials with nanometric sized particles (1 nm = 10^{-9} m) show interesting physical and chemical properties for different applications, including gas sensors [1–10].

Several synthesis methods are currently employed to obtain materials with nanometric particles and desired morphological features, like colloid, sol-gel, coprecipitation, ultrasonic spray, polymerization, and so forth [11–16]. For gas sensor applications, the morphology and a reduced particle size play an important role due to the increase of the specific surface area and, therefore, of the sensitivity, enhancing at the same time the chemical adsorption and the physical adsorption of the gases [17–20].

SnO_2, $LaFeO_3$, TiO_2, ZnO, In_2O_3, and WO_3, among other oxides, have been extensively used in gas sensor applications [21–25]. However, in recent years, trirutile-type oxides are of interest as gas sensors, because they show good electric response and chemical stability, as well as gas selectivity [26–28]. $CoSb_2O_6$ has shown, for example, very good performance as CO_2 and O_2 sensor, due to its morphology and particle size [29], and $ZnSb_2O_6$ has been found to be very suitable for detecting H_2S, due to its porosity [30].

In order to obtain the trirutile-type $CoSb_2O_6$ with specific size, porosity, and morphological features for gas sensing, a nonaqueous chemical method was used in this work, which

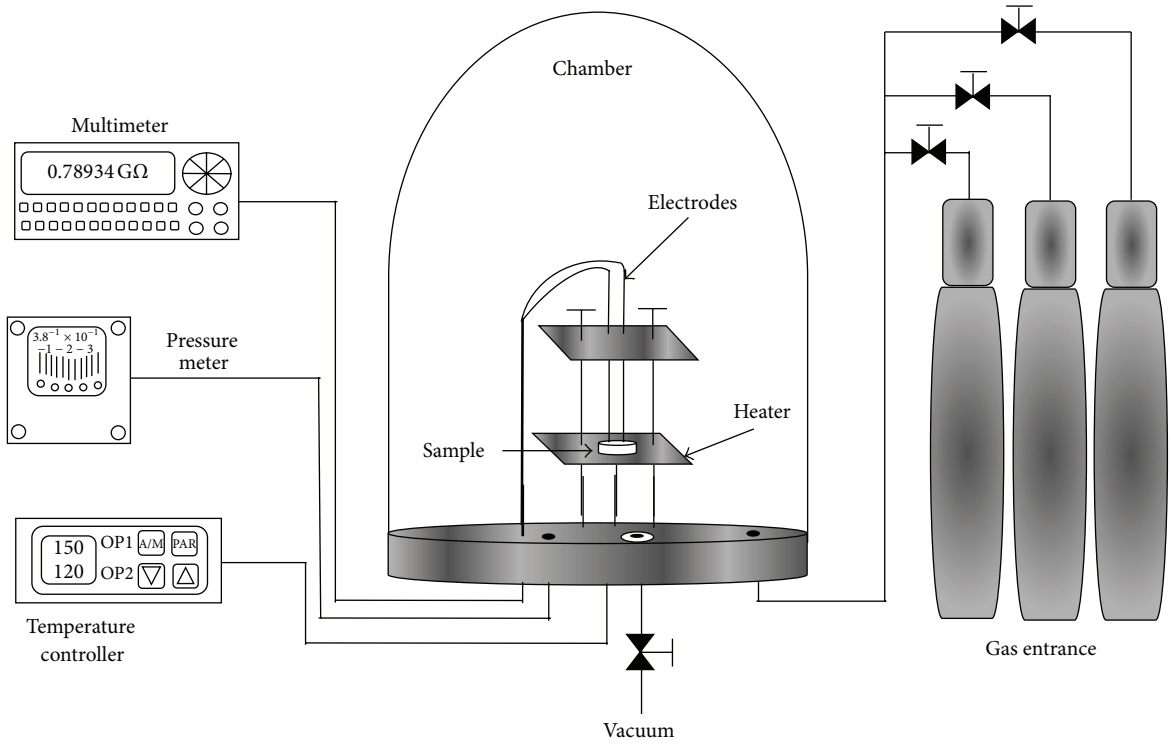

Figure 1: Arrangement employed for the sensitivity testing of $CoSb_2O_6$.

presented the additional advantage of not being expensive [31]. The material's characterization was made by scanning and transmission electron microscopies (SEM and TEM, resp.). The good sensitivity results of the obtained mesoporous $CoSb_2O_6$ nanoparticles in CO and C_3H_8 atmospheres support the use of these oxides as gas sensors.

2. Experimental Procedures

$CoSb_2O_6$ nanoparticles with trirutile-type structure were prepared employing a colloidal method [29]; however, in order to modify the microstructure, cobalt nitrate (Jalmek), antimony trichloride (Sigma-Aldrich), 4 mL of ethylenediamine (Sigma), and analytic grade ethanol (CTR) were employed in this work. The solvent was evaporated by means of a microwave oven (General Electric, model JES769WK) at a power of 70 W and applying pulses at 20–30 s intervals. After this, the precursor material was dried at 200°C during 8 h and calcined at 600°C at a heating rate of 100°C/h using a programmable muffle (Vulcan 3-550).

The crystallinity characterization was carried out at room temperature by means of Siemens D500 X-ray powder diffraction (XRD) system using a nickel filter and Cu$K\alpha$ radiation. A 2θ continuous diffraction scanning was performed from 20° to 70° and 1 s-steps of 0.02°.

The morphology of the calcined $CoSb_2O_6$ was characterized by means of a scanning electron microscopy (SEM) system (Jeol, model JSM-6390LV) in high vacuum and using the secondary electron emission. The particle size and morphology were analyzed with a transmission electron microscopy (TEM) system (Jeol, model JEM-2010) at a 200 kV acceleration voltage. Prior to this, the $CoSb_2O_6$ powder was dispersed in isopropyl alcohol by means of a sonicator during 5 min.

For the sensitivity tests, 0.5 g of $CoSb_2O_6$ powder was pressed at 15 ton during 90 min with a manual pressing machine (Simplex Ital Equip–25 tons). The obtained pellet, with a 12 mm diameter and a 0.5 mm thickness, was heated at 200°C during 1 h and set after that in a vacuum chamber at 10^{-3} Torr (see Figure 1).

The electrical resistance tests of the $CoSb_2O_6$ pellets were carried out in carbon monoxide (CO) and propane (C_3H_8) atmospheres to the concentrations 0, 5, 50, 100, 200, and 300 ppm at the temperatures 23, 150, 250, and 350°C. The gas detection sensitivity (S) was calculated according to the following formula [32–35]:

$$S = \frac{G_G - G_O}{G_O}, \tag{1}$$

where G_G and G_O are the electrical conductance of the $CoSb_2O_6$ pellets measured in gas (CO or C_3H_8) and air, respectively. The conductance was measured by means of a digital multimeter (Keithley, model 2001). Electrical contact with the pellet was made using silver electrodes, as shown in Figure 1.

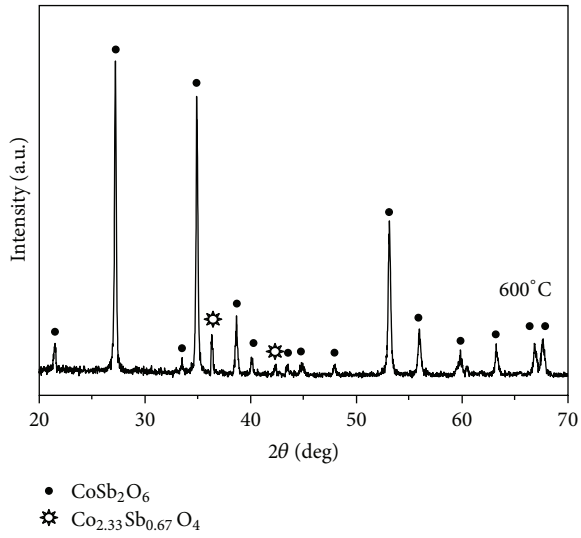

Figure 2: X-ray diffractogram of the calcined powder at 600°C, identifying the main and secondary phases: $CoSb_2O_6$ and $Co_{2.33}Sb_{0.67}O_4$, respectively.

3. Results and Discussion

3.1. X-Ray Diffraction Analysis. Figure 2 shows the diffractogram of the $CoSb_2O_6$ powders obtained at 600°C. The characteristic peaks of the oxide are clearly discernible and were identified by the JCPDF index-card 18-0403. According to this, $CoSb_2O_6$ is a trirutile-type oxide with tetragonal structure (cell parameters: a = 4.65 Å, b = 9.28 Å) and $P4_2/mnm$ space group [28]. The height and width of the peaks are indicative of a small particle size [36]; the presence of slight fluorescence shows high crystallinity. Further, a secondary phase was identified: $Co_{2.33}Sb_{0.67}O_4$ (JCPDF, 15-0517), located at $2\theta = 36.4^\circ$, 42.0°, and 61.1°. These results are consistent with other studies on the same oxide and similar ones (despite being synthesized by different methods and at higher temperatures) [26, 27, 29, 37]. We emphasize again the relative low temperature (600°C) at which the oxide was synthesized for this study.

3.2. Scanning Electron Microscopy Analysis. Three scanning electron microscopy (SEM) photomicrographs of the oxide's surface are depicted in Figure 3. Figure 3(a) shows the microstructure of $CoSb_2O_6$, where irregular particles of tetragonal morphology agglomerate on the whole porous surface. In Figure 3(b), tetragonal and cubic microcrystals are clearly discernible, showing also a multidirectional growth. The plane length of the cubic crystals is approximately 0.2–1.2 μm, ~0.735 μm on average, and has a standard deviation of ±0.2 μm. In the more magnified photomicrograph, Figure 3(c), the multidirectional growth of the tetrahedral crystals is more evident. It can be observed that every single face of the monocrystals is taken as a substrate for growing in different directions. The effect of ethylenediamine on the microstructure of materials has been reported in previous works [38]. The ethylenediamine acts as a template which is incorporated into the inorganic framework first and then escapes from it during the thermal treatment to form particles of desired morphologies [39]. Studies made with colloidal dispersions have obtained morphologies similar to those obtained in this study. In such cases, the morphologies have originated from the growth process of stable nuclei of the colloidal systems [40, 41], agreeing with the crystallization principles proposed by Lamer and Dinegar [42], which were described in three stages: the first one states that the concentration of the reagents in colloidal dispersions gradually increases; the second stage states that the concentration of the reagents reaches an oversaturation limit and the nucleation happens rapidly forming the nuclei of the crystals; and, finally, the third stage states that the growth of the crystals is originated by diffusion of the dissolved species to nuclei and thus their morphology is clear. Based on these principles, compounds with different morphologies can be obtained using colloidal methods.

3.3. Transmission Electron Microscopy Analysis. Three bright field transmission electron microscopy (TEM) photomicrographs of the oxide's surface are shown in Figure 4. The formation of the tetrahedral nanometric monocrystals is depicted in Figure 4(a). The particle size is 70–150 nm. The agglomeration of nanoparticles, joined by necks originated from particle coalescence, is depicted in Figures 4(b) and 4(c). Uniformly distributed mesopores on the nanoparticles' surface are discernible.

Size distribution of the nanoparticles and mesopores is shown in Figure 5. The estimated nanoparticle size is in the range 20–70 nm, ~41.1 nm on average, and has a standard deviation of ±12 nm. From TEM images, the mesopores diameter was estimated in the range 5–8.5 nm, ~6.5 nm on average, and has a standard deviation of ±0.81 nm. The diameter agrees with those obtained in other studies, despite using different synthesis methods [43–47].

3.4. Gas Sensing Properties. Figure 6 depicts the sensitivity of the mesoporous $CoSb_2O_6$ nanoparticles in terms of the CO concentrations and operating temperatures. At temperatures 23°C (ambient) and 150°C, no significant change on the sensitivity to CO is discernible (Figure 6(a)), but, at 250 and 350°C, a change was detected (Figure 6(b)). In particular, at 250°C, the gas sensitivity values calculated were 0, 0.10, 2.26, 3.80, and 5.10 in presence of 0, 5, 50, 100, and 200 ppm of CO, respectively, while, at 350°C, the gas sensitivity magnitude increased to 0, 0.61, 2.63, 4.70, and 7, under the same gas concentrations, respectively. Table 1 summarizes the obtained values. It can be seen that an increase in concentration and temperature meant an increase in sensitivity [48]. To explain this, it has been reported that the ionization states of the chemically adsorbed oxygen highly depend on temperature; at temperatures lower than 150°C, O_2^- species are present. However, at temperatures greater than that, the more reactive O^- and O^{2-} species are predominant [49, 50]. The formation at high temperature of the latter species means a rise in the gas-solid interaction in the presence of CO [51], causing an increase in the sensitivity.

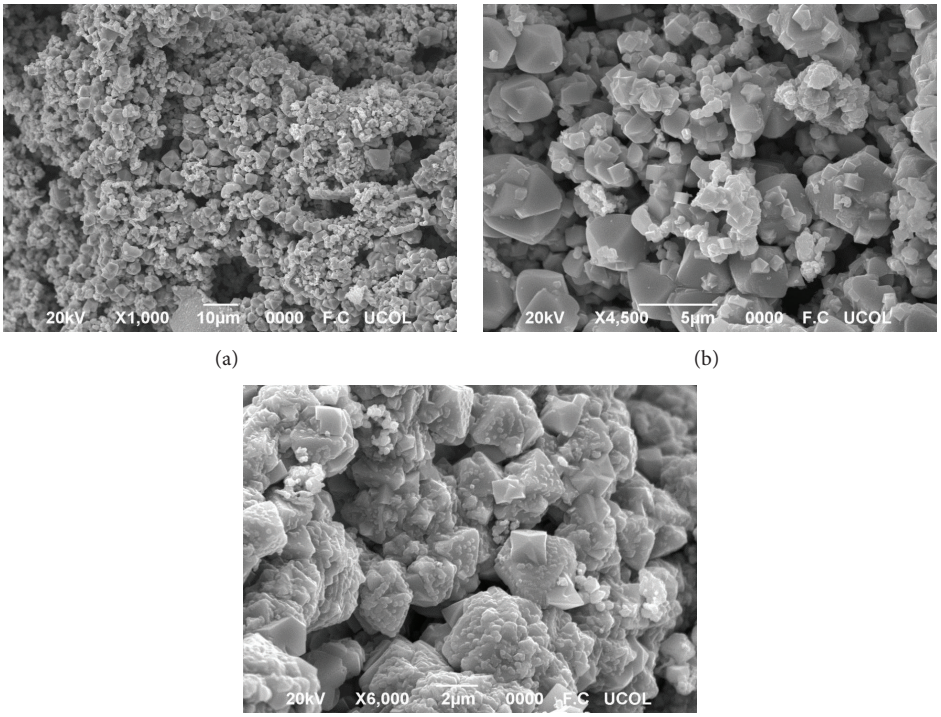

(a) (b)

(c)

Figure 3: SEM images of $CoSb_2O_6$ at several magnifications: (a) 1000x, (b) 4500x, and (c) 6000x.

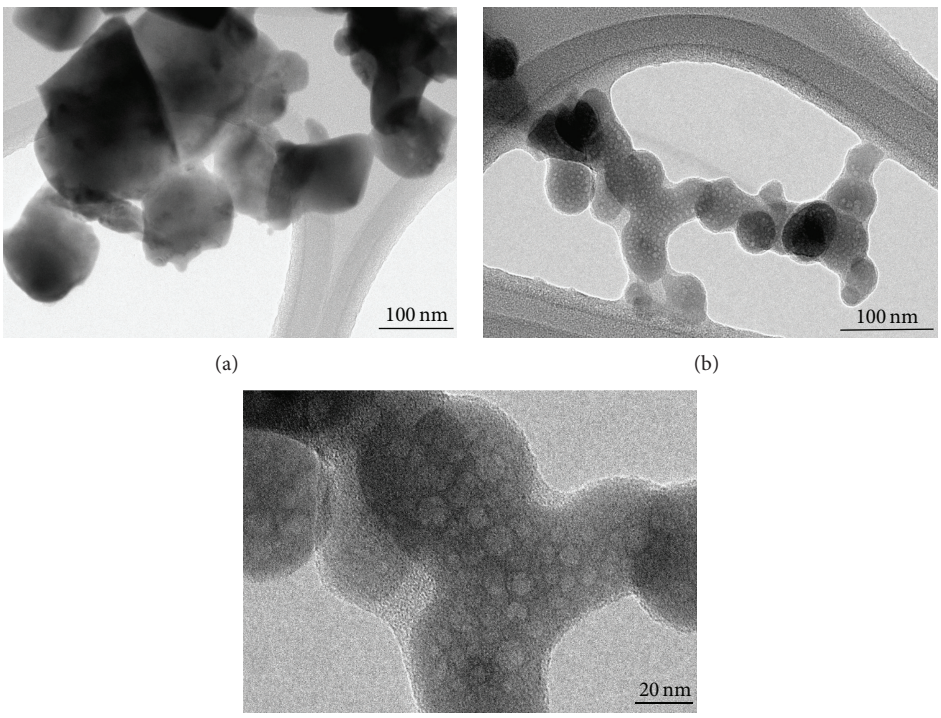

(a) (b)

(c)

Figure 4: Bright field TEM photomicrographs of $CoSb_2O_6$ showing (a) cubes and tetrahedral pyramids and (b-c) mesoporous nanoparticles.

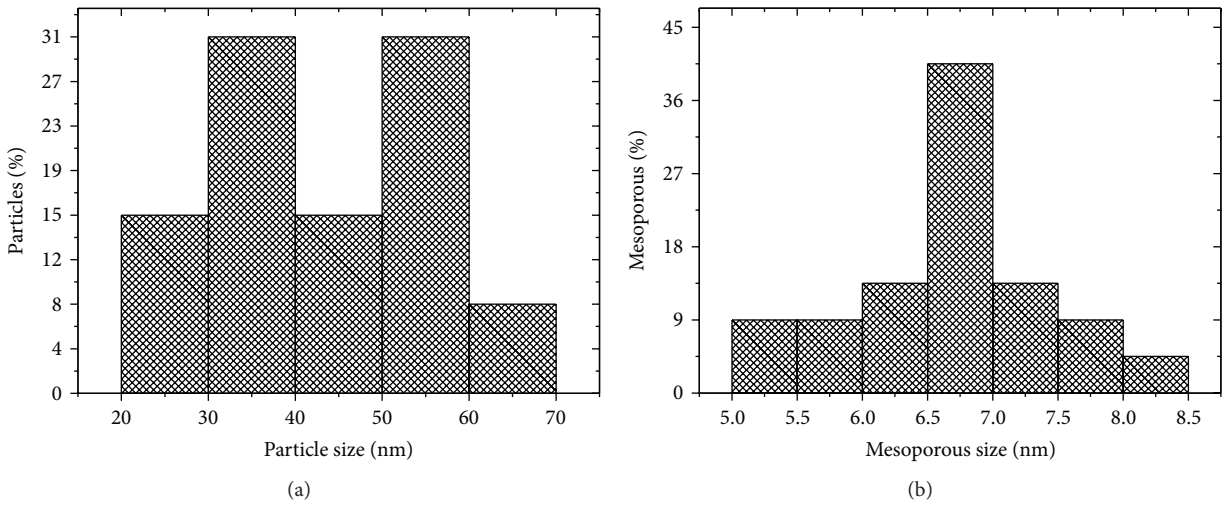

FIGURE 5: Size distribution of $CoSb_2O_6$: (a) nanoparticles and (b) mesopores.

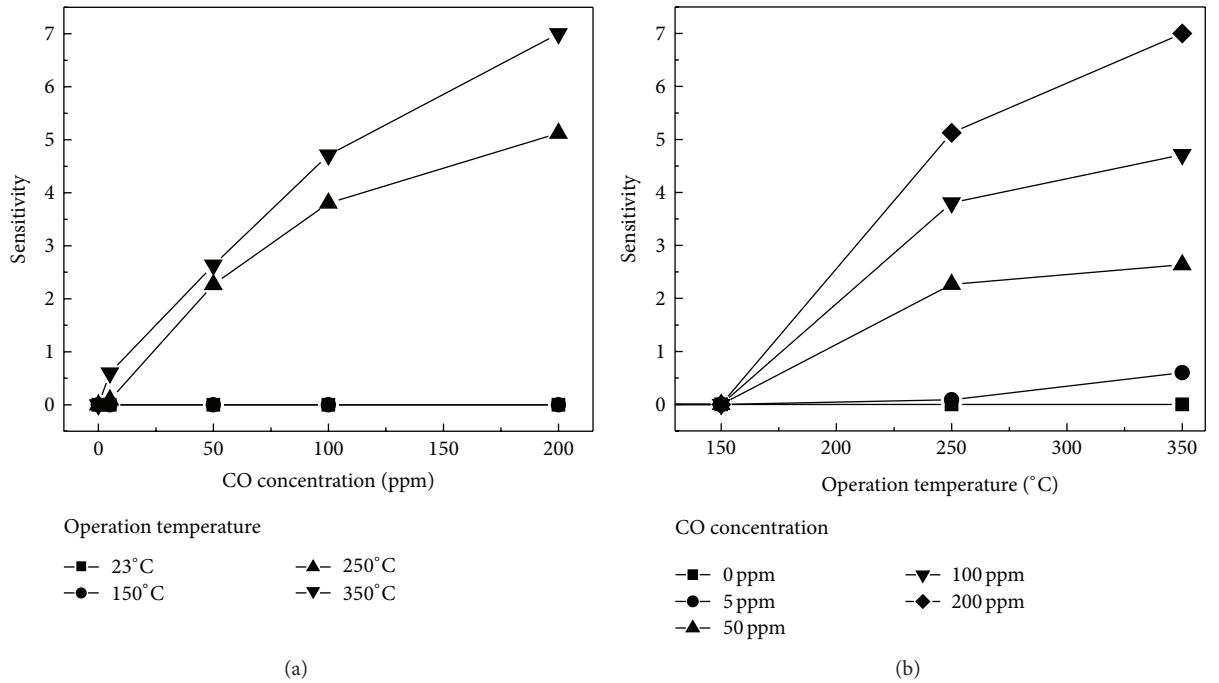

FIGURE 6: Gas sensitivity of $CoSb_2O_6$ oxide as a function of (a) CO concentration and (b) CO operation temperature.

TABLE 1: Sensitivity values of $CoSb_2O_6$ in CO atmospheres.

Temperature (°C)	Concentration CO (ppm)	Sensitivity (S)	Temperature (°C)	Concentration CO (ppm)	Sensitivity (S)
250	0	0	350	0	0
	5	0.10		5	0.61
	50	2.26		50	2.63
	100	3.80		100	4.70
	200	5.10		200	7.00

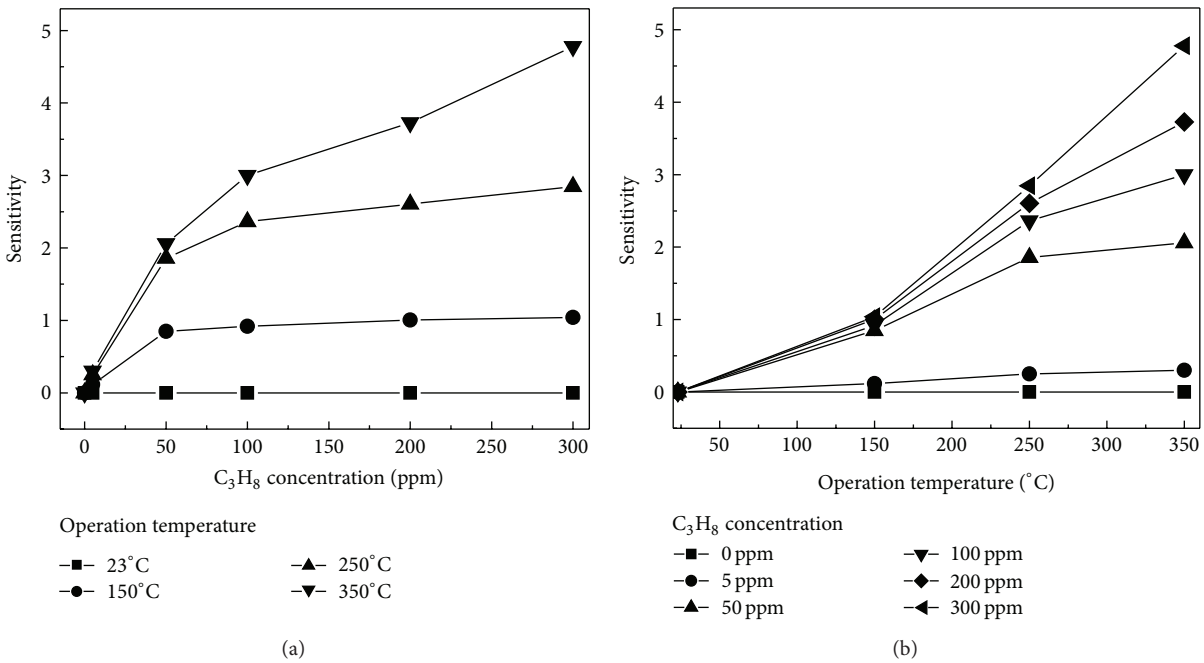

Figure 7: Gas sensitivity of $CoSb_2O_6$ oxide as a function of (a) C_3H_8 concentration and (b) C_3H_8 operation temperature.

When the CO molecules make contact with the surface of the $CoSb_2O_6$ pellets at moderate temperatures (250°C and 350°C), the adsorbed CO reacts with the oxygen anions chemisorbed on the surface, yielding CO_2 and a release of electrons back into the conduction band [48, 52, 53]. The mechanism of CO adsorption greatly depends on the temperature, and at least one of the following reactions may occur at different operating temperatures [17, 52, 53]:

$$2CO\,(gas) + O_2^{-}\,(ads) \longrightarrow 2CO_2 + e^{-} \quad (2)$$

$$CO\ (gas) + O^{-}\,(ads) \longrightarrow CO_2 + e^{-} \quad (3)$$

$$CO\,(gas) + O^{2-}\,(ads) \longrightarrow CO_2 + 2e^{-} \quad (4)$$

where the suffix (ads) denotes the adsorbed species [17, 52]. In this case, the electrons present in the reactions combine with charge carriers in the oxide's valence band. According to these chemical paths, the gas-sensing mechanism in semiconductor materials is based on the electric resistance change (i.e., conductance) produced by the electron transfer that takes place during the chemical adsorption [18, 29]. In the presence of a reducing electron-donator species, like CO, the whole concentration diminishes and the resistance increases, causing changes in the material's response.

The gas sensitivity as a function of the propane (C_3H_8) concentrations and operating temperatures are shown in Figures 7(a) and 7(b), respectively. $CoSb_2O_6$ nanoparticles are sensible to both propane gas concentration and operation temperature, even at 150°C. At this temperature, the gas sensitivity values of $CoSb_2O_6$ were 0, 0.12, 0.85, 0.92, 1.00, and 1.04 under 0, 5, 50, 100, 200, and 300 ppm of propane, respectively, while, at 250°C, the pellets exhibited higher sensitivity values around 0, 0.22, 1.8, 2.1, 2.4, and 2.7 under the same gas concentrations, respectively. However, at 350°C, the $CoSb_2O_6$ nanoparticles exhibited greater sensitivity values around 0, 0.23, 2, 3, 3.7, and 4.8 in the same propane concentrations. The sensitivity increased, because more desorption reactions take place when the propane concentration rises [48, 54]. In addition, the sensitivity increases more uniformly in propane atmosphere. This can be accounted for from the rise of the oxygen's adsorption at high temperatures [54]. At room temperature, no resistance changes are recorded, because the thermal energy is not enough to produce the desorption reactions. Our findings are in agreement with [50]. In addition, we have found that, when the test gases were removed from the vacuum chamber, the oxide's sensitivity decreased, as in a reversed process. Table 2 summarizes the findings.

According to these results, the detection mechanism of C_3H_8 at 250°C and 350°C is not obvious. However, some authors have investigated other materials that detect propane at different gas concetraciones and operating temperatures [32, 33, 54]. Then, comparing our results with such studies, the sensitivity of our oxide is far better. For example, [32, 33] report a maximum sensitivity of 0.7 and 0.4 for a propane concentration of 300 ppm at 300°C, using SnO_2 and ZnO, respectively. The value obtained in this work, $S = 4.8$ at 350°C, and the same concentration of C_3H_8, speaks of the important role played by the nanometric particle size, which we attribute to the synthesis route. As mentioned, $CoSb_2O_6$ nanoparticles have been studied as potential gas sensors, due to their ability to detect variations in the concentration of gases, such as CO_2 and O_2 [29]. Now, in the present work, it has been found that $CoSb_2O_6$ nanoparticles exhibit very good gas sensitivity in CO and propane atmospheres, even at relatively low temperatures.

Table 2: Sensitivity values of $CoSb_2O_6$ in C_3H_8 atmospheres.

Temperature (°C)	Concentration C_3H_8 (ppm)	Sensitivity (S)	Temperature (°C)	Concentration C_3H_8 (ppm)	Sensitivity (S)
250	0	0	350	0	0
	5	0.22		5	0.23
	50	1.8		50	2
	100	2.1		100	3
	200	2.4		200	3.7
	300	2.7		300	4.8

Due to the fact that the microstructure of a material used as a gas detector is considered to be of great importance for satisfactory operation, when the particle size is nanometric, the sensitivity can be substantially improved [20], because the average crystal size is smaller than twice the thickness of the charged outer layer (L_S), which is defined as in [18, 29]:

$$L_S = L_D \sqrt{\frac{eV_S^2}{kT}}, \tag{5}$$

where L_D is the Debye length, e is the charge of the electron, V_S is the potential of the surface, k is the Boltzmann constant, and T is the temperature. Usually, L_S values are between 1 and 100 nm [18].

According to some authors (e.g., [55]), the charged outer layer mainly depends on the gas pressure and concentrations. Owing to this, the conductivity will strongly depend on the crystal size (D), yielding three possible scenarios [18]: (1) if $D \gg 2L_S$, the conductivity is limited by the Schottky barrier at the particle border; thus, the gas detection does not depend on the particle size; (2) if $D = 2L_S$, the conductivity and the gas sensing properties depend on the formation of necks built by crystals; (3) if $D < 2L_S$, the conductivity depends on the crystal size [18, 20, 55]. Based on these three scenarios, the known physical fact that the smaller the particle size (accomplished in our case during the synthesis process), the greater the surface area obtained can be neatly used in the gas sensors field.

4. Conclusions

The trirutile-type oxide was synthesized by a convenient method which allowed using the material at low temperatures. The mesoporous $CoSb_2O_6$ nanoparticles are highly sensitive to CO and C_3H_8 operating at relative low temperatures. It has been observed that when increasing temperature and concentration, the sensitivity rises. The maximum sensitivity was reached for the concentrations 200 and 300 ppm at 350°C. The success using $CoSb_2O_6$ as a gas sensor is attributed to the nanometric particle size.

Conflict of Interests

The authors declare that there is no conflict of interests regarding the publication of this paper.

Acknowledgments

Héctor Guillén-Bonilla and Lorenzo Gildo-Ortiz express their gratitude to Consejo Nacional de Ciencia y Tecnología (CONACyT) for the scholarships received. The technical support received from Darío Pozas Zepeda and Miguel Ángel Luna Arias is also appreciated. This work was partially supported by Project no. 784-12 FRABA.

References

[1] C. N. R. Rao and A. K. Cheetham, "Science and technology of nanomaterials: current status and future prospects," *Journal of Materials Chemistry*, vol. 11, no. 12, pp. 2887–2894, 2001.

[2] W. Chen, H. Gan, W. Zhang, and Z. Mao, "Hydrothermal synthesis and hydrogen sensing properties of nanostructured SnO_2 with different morphologies," *Journal of Nanomaterials*, vol. 2014, Article ID 291273, 7 pages, 2014.

[3] R. Seoudi and D. A. Said, "Studies on the effect of the capping materials on the spherical gold nanoparticles catalytic activity," *World Journal of Nano Science and Engineering*, vol. 1, no. 2, pp. 51–61, 2011.

[4] S. Vallejos, I. Gràcia, E. Figueras, and C. Cané, "Catalyst-free vapor-phase method for direct integration of gas sensing nanostructures with polymeric transducing platforms," *Journal of Nanomaterials*, vol. 2014, Article ID 932129, 9 pages, 2014.

[5] P. Slobodian, P. Riha, P. Cavallo et al., "Highly enhanced vapor sensing of multiwalled carbon nanotube network sensors by *n*-butylamine functionalization ," *Journal of Nanomaterials*, vol. 2014, Article ID 589627, 8 pages, 2014.

[6] S. D. Ramamurthi, Z. Xu, and D. A. Payne, "Nanometer-sized ZrO_2 particles prepared by a sol-emulsion-gel method," *Journal of the American Ceramic Society*, vol. 73, no. 9, pp. 2760–2763, 1990.

[7] Z. Chen, E. Shi, W. Li, Y. Zheng, N. Wu, and W. Zhong, "Particle size comparison of hydrothermally synthesized cobalt and zinc aluminate spinels," *Journal of the American Ceramic Society*, vol. 85, no. 12, pp. 2949–2955, 2002.

[8] V. Polshettiwar, B. Baruwati, and R. S. Varma, "Self-assembly of metal oxides into three-dimensional nanostructures: synthesis and application in catalysis," *ACS Nano*, vol. 3, no. 3, pp. 728–736, 2009.

[9] G. Wang, X. Gou, J. Horvat, and J. Park, "Facile synthesis and characterization of iron oxide semiconductor nanowires for gas sensing application," *The Journal of Physical Chemistry C*, vol. 112, no. 39, pp. 15220–15225, 2008.

[10] S. Yang and L. Gao, "Synthesis and characterization of porous single-crystalline titanium dioxide nanorods," *Journal of the American Ceramic Society*, vol. 89, no. 2, pp. 720–723, 2006.

[11] S. Bose and Y. Wu, "Synthesis of Al_2O_3-CeO_2 mixed oxide nano-powders," *Journal of the American Ceramic Society*, vol. 88, no. 7, pp. 1999–2002, 2005.

[12] R. N. Das, "Nanocrystalline ceramics from sucrose process," *Materials Letters*, vol. 47, no. 6, pp. 344–350, 2001.

[13] M. Montero, T. Molina, M. Szafran, R. Moreno, and M. I. Nieto, "Alumina porous nanomaterials obtained by colloidal processing using D-fructose as dispersant and porosity promoter," *Ceramics International*, vol. 38, no. 4, pp. 2779–2784, 2012.

[14] J. Zhang, Q. Xu, H. Tanaka, M. Iwasa, and D. Jiang, "Improvement of the dispersion of Al_2O_3 slurries using EDTA-4Na," *Journal of the American Ceramic Society*, vol. 89, no. 4, pp. 1440–1442, 2006.

[15] O. Vasylkiv and Y. Sakka, "Nanoexplosion synthesis of multimetal oxide ceramic nanopowders," *Nano Letters*, vol. 5, no. 12, pp. 2598–2604, 2005.

[16] S.-J. Lee and W. M. Kriven, "Crystallization and densification of nano-size amorphous cordierite powder prepared by a PVA solution-polymerization route," *Journal of the American Ceramic Society*, vol. 81, no. 10, pp. 2605–2612, 1998.

[17] M.-I. Baraton and L. Merhari, "Electrical behavior of semiconducting nanopowders versus environment," *Reviews on Advanced Materials Science*, vol. 4, no. 1, pp. 15–24, 2003.

[18] V. E. Bochenkov and G. B. Sergeev, "Preparation and chemiresistive properties of nanostructured materials," *Advances in Colloid and Interface Science*, vol. 116, no. 1–3, pp. 245–254, 2005.

[19] S. C. Yeow, W. L. Ong, A. S. W. Wong, and G. W. Ho, "Template-free synthesis and gas sensing properties of well-controlled porous tin oxide nanospheres," *Sensors and Actuators, B: Chemical*, vol. 143, no. 1, pp. 295–301, 2009.

[20] N. Yamazoe, "New approaches for improving semiconductor gas sensors," *Sensors and Actuators: B Chemical*, vol. 5, no. 1–4, pp. 7–19, 1991.

[21] M. Fleischer and H. Meixner, "Fast gas sensors based on metal oxides which are stable at high temperatures," *Sensors and Actuators B: Chemical*, vol. 43, no. 1–3, pp. 1–10, 1997.

[22] M. C. Carotta, M. A. Butturi, G. Martinelli, Y. Sadaoka, P. Nunziante, and E. Traversa, "Microstructural evolution of nanosized $LaFeO_3$ powders from the thermal decomposition of a cyano-complex for thick film gas sensors," *Sensors and Actuators, B: Chemical*, vol. 44, no. 1–3, pp. 590–594, 1997.

[23] C. R. Michel, E. L. Mena, A. H. M. Preciado, and E. de León, "Improvement of the gas sensing behavior in nanostructured $Gd_{0.9}Sr_{0.1}CoO_3$ by addition of silver," *Materials Science and Engineering B: Solid-State Materials for Advanced Technology*, vol. 141, no. 1-2, pp. 1–7, 2007.

[24] Z. Jin, H.-J. Zhou, Z.-L. Jin, R. F. Savinell, and C.-C. Liu, "Application of nano-crystalline porous tin oxide thin film for CO sensing," *Sensors and Actuators B: Chemical*, vol. 52, no. 1-2, pp. 188–194, 1998.

[25] L. Wang, A. Teleki, S. E. Pratsinis, and P. I. Gouma, "Ferroelectric WO_3 nanoparticles for acetone selective detection," *Chemistry of Materials*, vol. 20, no. 15, pp. 4794–4796, 2008.

[26] D. Larcher, A. S. Prakash, L. Laffont et al., "Reactivity of antimony oxides and MSb_2O_6 (M = Cu, Ni, Co), trirutile-type phases with metallic lithium," *Journal of the Electrochemical Society*, vol. 153, no. 9, pp. A1778–A1787, 2006.

[27] H. Mizoguchi and P. M. Woodward, "Electronic structure studies of main group oxides possessing edge-sharing octahedra: implications for the design of transparent conducting oxides," *Chemistry of Materials*, vol. 16, no. 25, pp. 5233–5248, 2004.

[28] A. Jamal, M. M. Rahman, S. B. Khan et al., "Cobalt doped antimony oxide nano-particles based chemical sensor and photo-catalyst for environmental pollutants," *Applied Surface Science*, vol. 261, pp. 52–58, 2012.

[29] C. R. Michel, H. Guillén-Bonilla, A. H. Martínez-Preciado, and J. P. Morán-Lázaro, "Synthesis and gas sensing properties of nanostructured $CoSb_2O_6$ microspheres," *Sensors and Actuators B: Chemical*, vol. 143, no. 1, pp. 278–285, 2009.

[30] J. Tamaki, Y. Yamada, Y. Yamamoto, M. Matsuoka, and I. Ota, "Sensing properties to dilute hydrogen sulfide of $ZnSb_2O_6$ thick-film prepared by dip-coating method," *Sensors and Actuators, B: Chemical*, vol. 66, no. 1, pp. 70–73, 2000.

[31] C. R. Michel, A. H. Martínez-Preciado, J. P. Morán-Lázaro, and H. Guillén-Bonilla, "CO_2 detection in nanostructured $CoSb_2O_6$ prepared by a non-aqueous colloidal method," *ECS Transactions*, vol. 25, no. 31, pp. 49–51, 2010.

[32] H. Gómez-Pozos, J. L. González-Vidal, G. A. Torres et al., "Chromium and ruthenium-doped zinc oxide thin films for propane sensing applications," *Sensors*, vol. 13, no. 3, pp. 3432–3444, 2013.

[33] H. Gómez-Pozos, J. L. González-Vidal, G. A. Torres, M. de la Luz Olvera, and L. Castañeda, "Physical characterization and effect of effective surface area on the sensing properties of tin dioxide thin solid films in a propane atmosphere," *Sensors*, vol. 14, no. 1, pp. 403–415, 2013.

[34] J.-J. Ho, Y. K. Fang, K. H. Wu et al., "High sensitivity ethanol gas sensor integrated with a solid-state heater and thermal isolation improvement structure for legal drink-drive limit detecting," *Sensors and Actuators, B: Chemical*, vol. B50, no. 3, pp. 227–233, 1998.

[35] L. L. Fields, J. P. Zheng, Y. Cheng, and P. Xiong, "Room-temperature low-power hydrogen sensor based on a single tin dioxide nanobelt," *Applied Physics Letters*, vol. 88, no. 26, Article ID 263102, 3 pages, 2006.

[36] E. Delgado and C. R. Michel, "CO_2 and O_2 sensing behavior of nanostructured barium-doped $SmCoO_3$," *Materials Letters*, vol. 60, no. 13-14, pp. 1613–1616, 2006.

[37] C. R. Michel, A. H. Martínez, and S. Jiménez, "Gas sensing response of nanostructured trirutile-type $CoSb_2O_6$ synthesized by solution-polymerization method," *Sensors and Actuators B: Chemical*, vol. 132, no. 1, pp. 45–51, 2008.

[38] H. Guillén-Bonilla, J. Reyes-Gomez, A. Guillén-Bonilla et al., "Synthesis and characterization of $MgSb_2O_6$ trirutile-type in low presence concentrations of ethylenediamine," *Journal of Chemistry and Chemical Engineering*, vol. 7, pp. 395–401, 2013.

[39] Z.-X. Deng, C. Wang, X.-M. Sun, and Y.-D. Li, "Structure-directing coordination template effect of ethylenediamine in formations of ZnS and ZnSe nanocrystallites via solvothermal route," *Inorganic Chemistry*, vol. 41, no. 4, pp. 869–873, 2002.

[40] E. Matijevic, "Uniform inorganic colloid dispersions. Achievements and challenges," *Langmuir*, vol. 10, no. 1, pp. 8–16, 1994.

[41] E. Matijević, "Monodispersed colloids: art and science," *Langmuir*, vol. 2, no. 1, pp. 12–20, 1986.

[42] V. K. Lamer and R. H. Dinegar, "Theory, production and mechanism of formation of monodispersed hydrosols," *Journal of the American Chemical Society*, vol. 72, no. 11, pp. 4847–4854, 1950.

[43] W. H. Lai, L. G. Teoh, Y. H. Su, J. Shieh, and M. H. Hon, "Effect of calcination on crystallinity for nanostructured development of wormhole-like mesoporous tungsten oxide," *Journal of the American Ceramic Society*, vol. 90, no. 12, pp. 4073–4075, 2007.

[44] M. Mougenot, M. Lejeune, J. F. Baumard et al., "Ink jet printing of microdot arrays of mesostructured silica," *Journal of the American Ceramic Society*, vol. 89, no. 6, pp. 1876–1882, 2006.

[45] S. Costacurta, L. Biasetto, E. Pippel, J. Woltersdorf, and P. Colombo, "Hierarchical porosity components by infiltration of a ceramic foam," *Journal of the American Ceramic Society*, vol. 90, no. 7, pp. 2172–2177, 2007.

[46] L. Lu and A. Eychmüller, "Ordered macroporous bimetallic nanostructures: design, characterization, and applications," *Accounts of Chemical Research*, vol. 41, no. 2, pp. 244–253, 2008.

[47] Y. Shimizu, T. Hyodo, and M. Egashira, "Meso- to macroporous oxides as semiconductor gas sensors," *Catalysis Surveys from Asia*, vol. 8, no. 2, pp. 127–135, 2004.

[48] G. Bläser, T. Rühl, C. Diehl, M. Ulrich, and D. Kohl, "Nanostructured semiconductor gas sensors to overcome sensitivity limitations due to percolation effects," *Physica A: Statistical Mechanics and its Applications*, vol. 266, no. 1–4, pp. 218–223, 1999.

[49] M. Siemons and U. Simon, "High throughput screening of the sensing properties of doped $SmFeO_3$," *Solid State Phenomena*, vol. 128, pp. 225–236, 2007.

[50] S. C. Chang, "Oxygen chemisorption on tin oxide: correlation between electrical conductivity and EPR measurements,," *Journal of Vacuum Science & Technology*, vol. 17, no. 1, pp. 366–369, 1979.

[51] N. N. Toan, S. Saukko, and V. Lantto, "Gas sensing with semiconducting perovskite oxide $LaFeO_3$," *Physica B*, vol. 327, no. 2–4, pp. 279–282, 2003.

[52] C. R. Michel, "CO and CO_2 gas sensing properties of mesoporous $CoAl_2O_4$," *Sensors and Actuators B: Chemical*, vol. 147, no. 2, pp. 635–641, 2010.

[53] C.-C. Hsiao and L.-S. Luo, "A rapid process for fabricating gas sensors," *Sensors*, vol. 14, no. 7, pp. 12219–12232, 2014.

[54] L. Gildo-Ortiz, H. Guillén-Bonilla, J. Santoyo-Salazar et al., "Low-temperature synthesis and gas sensitivity of perovskite-type $LaCoO_3$ nanoparticles," *Journal of Nanomaterials*, vol. 2014, Article ID 164380, 8 pages, 2014.

[55] C. R. Michel, E. Delgado, and A. H. Martínez, "Evidence of improvement in gas sensing properties of nanostructured bismuth cobaltite prepared by solution-polymerization method," *Sensors and Actuators, B: Chemical*, vol. 125, no. 2, pp. 389–395, 2007.

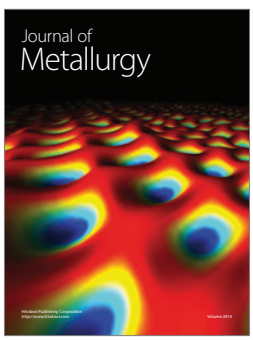

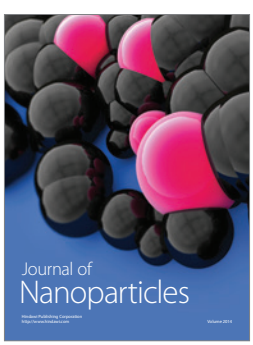

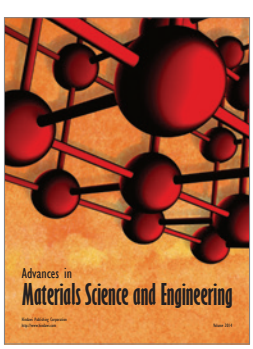

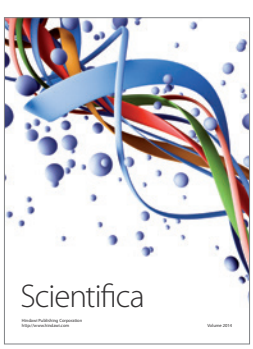

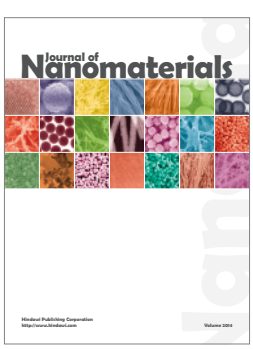

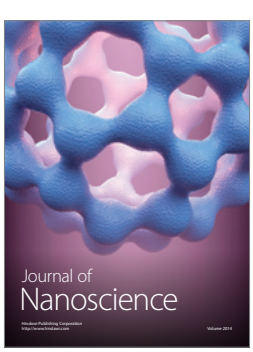

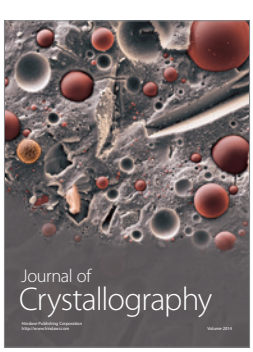

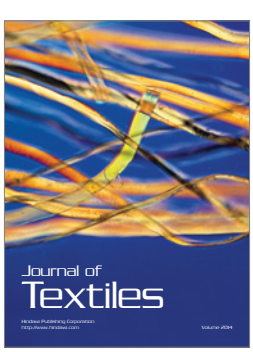

Hindawi

Submit your manuscripts at
http://www.hindawi.com